Numerical method for integrodifferential generalized Langevin and master equations

Joshua Wilkie
Department of Chemistry, Simon Fraser University, Burnaby, British Columbia, Canada V5A 1S6
(Received 5 May 2003; published 12 August 2003)

We show that the integrodifferential generalized Langevin and non-Markovian master equations can be transformed into larger sets of ordinary-differential equations. On the basis of this transformation we develop a numerical method for solving such integrodifferential equations. Physically motivated example calculations are performed to demonstrate the accuracy and convergence of the method.

DOI: 10.1103/PhysRevE.68.027701 PACS number(s): 05.10.−a, 02.60.−x, 05.30.−d, 05.40.−a

Generalized Langevin equations [1] and non-Markovian master equations [2–4], which arise in the treatment of systems interacting with environmental degrees of freedom, often have an integrodifferential form. Unlike ordinary-differential equations that can be readily solved using Runge-Kutta, predictor-corrector, and other well known numerical schemes [5], there are no general methods for solving equations of integrodifferential type. Here, we show that these integrodifferential equations can be converted to ordinary-differential equations at the expense of introducing a new time variable which is treated as if it is of spatial type. (Similar schemes are employed to numerically solve the Schrödinger equation for time-dependent Hamiltonians [6] and as analytical tools [7]. There is also some resemblance to the schemes for solving the integrodifferential equations of viscoelasticity [8].) We then develop a numerical method based on this exact transformation and show that it can be used to accurately solve a variety of physically motivated examples.

Neglecting inhomogeneous terms resulting from noise, for simplicity, the generalized Langevin equations [1] for position $q(t)$ and momentum $p(t)$ of a damped oscillator in one dimension can be expressed in the form

$$dq(t)/dt = p(t)/m, \tag{1}$$

$$dp(t)/dt = -m\omega^2 q(t) - \int_{-\infty}^{t} \gamma(t,t')p(t')dt', \tag{2}$$

where m and ω are the mass and frequency of the oscillator and $\gamma(t,t')$ is the memory function. Defining a spacelike time variable u and a function

$$\chi(t,u) = f(u)\int_{-\infty}^{t} \gamma(t+u,t')p(t')dt', \tag{3}$$

it can be verified by direct substitution that $p(t)$ and $\chi(t,u)$ satisfy the following ordinary-differential equations:

$$dp(t)/dt = -m\omega^2 q(t) - \chi(t,0), \tag{4}$$

$$d\chi(t,u)/dt = f(u)\gamma(t+u,t)p(t) + \frac{\partial \chi(t,u)}{\partial u} - \frac{f'(u)}{f(u)}\,\chi(t,u). \tag{5}$$

Here, we have introduced a differentiable damping function $f(u)$ [with $f(0)=1$] which plays a useful role in the numerical scheme we will introduce to solve the ordinary-differential equations (1), (4), and (5). [Note that $f'(u) = df(u)/du$.]

Neglecting inhomogeneous terms, non-Markovian master equations [2–4] can be written in the form

$$d\rho(t)/dt = -i[H(t),\rho(t)] - \int_{-\infty}^{t} K(t,t')\rho(t')dt', \tag{6}$$

where $\rho(t)$ is the time-evolving reduced density matrix of the subsystem, $H(t)$ is an effective Hamiltonian, and $K(t,t')$ is a memory operator. (We employ units such that $\hbar = 1$.) Defining an operator

$$\chi(t,u) = f(u)\int_{-\infty}^{t} K(t+u,t')\rho(t')dt', \tag{7}$$

it can be verified by direct substitution that $\rho(t)$ and $\chi(t,u)$ satisfy ordinary-differential equations

$$d\rho(t)/dt = -i[H(t),\rho(t)] - \chi(t,0), \tag{8}$$

$$d\chi(t,u)/dt = f(u)K(t+u,t)\rho(t) + \frac{\partial \chi(t,u)}{\partial u} - \frac{f'(u)}{f(u)}\,\chi(t,u). \tag{9}$$

Here $f(u)$ is again a differentiable damping function such that $f(0)=1$.

Thus, the integrodifferential Langevin equations (1) and (2) can be expressed in the ordinary-differential forms (1), (4), and (5), and the integrodifferential master equation (6) can be expressed as the ordinary-differential equations (8) and (9). To exploit these transformed equations as a practical numerical scheme, we must discretize the u variable on a grid of points so that the number of ordinary-differential equations is finite. Once this is achieved, the ordinary-differential equations can be solved using standard techniques [5]. We use an eighth-order Runge-Kutta routine [10] in our calculations.

To minimize the number of grid points, we choose a damping function $f(u)$ that decreases rapidly with u. In the calculations reported here, we used $f(u) = e^{-gu^2}$. In practice,

fewer grid points are needed for positive u than for negative u, and we found that the points $u_j=(-n+l+j)\Delta u$ for $j=1,\ldots,n$ worked well when we chose $l=\mathrm{int}(0.338n)$. Here, $u_n=l\Delta u$ is the largest positive u value. While accurate solutions can be obtained for almost any nonzero value of g, we found the most rapid convergence when values were optimized for the type of equation. Hence, g is specified differently below for each type of equation. To complete the numerical method, we need a representation of the partial derivative with respect to u on the grid. This could be performed via fast Fourier transform techniques [5]. We chose instead to employ a matrix representation

$$\left(\frac{\partial}{\partial u}\right)_{j,k}=\frac{(-1)^{j-k}}{(j-k)\Delta u}, \tag{10}$$

which is known as the sinc-DVR (discrete variable representation) [9]. A DVR is a complete set of basis functions, associated with a specific grid of points, in which functions of the variable are diagonal and derivatives have simple matrix representations [9]. DVRs are often used in multidimensional quantum mechanical scattering theory calculations [9]. In the sinc-DVR [9], which is associated with an equidistantly spaced grid on $(-\infty,\infty)$, partial derivatives can thus be evaluated with a sum

$$\left(\frac{\partial X(t,u)}{\partial u}\right)_{u=u_j}=\sum_{k=1}^{n}\frac{(-1)^{j-k}}{(j-k)\Delta u}X(t,u_k) \tag{11}$$

for any function or operator $X(t,u)$. In our calculations, we chose Δu to be equal to the time interval Δt between output from the Runge-Kutta routine.

We now discuss the applications of the above numerical method to specific models. For the generalized Langevin equation, we chose an initial value problem [i.e., $\gamma(t,t')=0$ for $t<t'$ and $\gamma(t,t')=W(t-t')$ for $t\geqslant t'$], where $W(t)$ has one of the following forms

$$W(t)=e^{-4t}, \tag{12}$$

$$W(t)=\frac{1}{9}\frac{e^{-t}-e^{-10t}}{1-e^{-t}}=\frac{1}{9}\sum_{j=1}^{9}e^{-jt}, \tag{13}$$

$$W(t)=2e^{-2t}-e^{-t}, \tag{14}$$

$$W(t)=3e^{-2t}-2.8e^{-t}+0.8e^{-t/2}, \tag{15}$$

which are displayed graphically in Fig. 1. The solid curve is given by (12), the dashed curve is given by Eq. (13), the short-dashed curve is given by Eq. (14) and the dotted curve is given by Eq. (15). These memory functions were chosen to roughly represent the various functional forms that can occur physically [1] and for ease in obtaining exact solutions. The constants appearing in Eqs. (1), (4), and (5) are chosen as $m=1$ and $\omega^2=10$. Figure 2 shows the functional form of the exact solutions $q(t)$ (solid curve) and $p(t)$ (dashed curve), which evolve from initial conditions $q(0)=1$ and $p(0)=0.1$, for memory function (12) over a time scale of 20 units

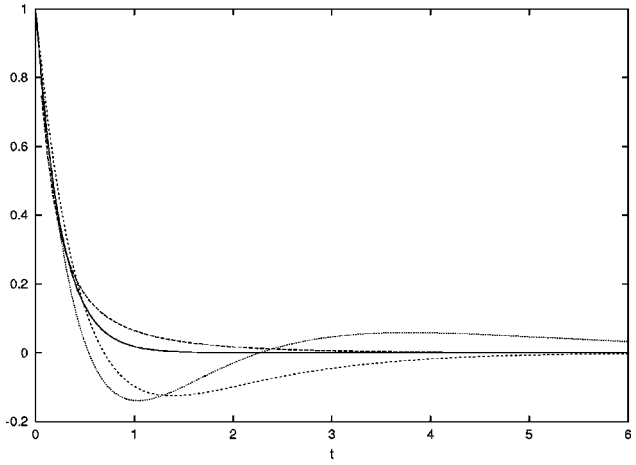

FIG. 1. Memory functions $W(t)$ plotted against time.

with $\Delta t=0.04$. Solutions for the other memory functions (and the same initial conditions) are similar in appearance. These exact solutions were obtained by exploiting the fact that the above memory functions are sums of exponentials (i.e., $W(t)=\Sigma_{j=1}^{\infty}a_je^{-b_jt}$) from which it follows that one may write

$$dp(t)/dt=-m\omega^2q(t)-\sum_{j=1}^{\infty}a_je^{-b_jt}y_j(t), \tag{16}$$

$$dy_j(t)/dt=e^{b_jt}p(t) \tag{17}$$

for $j=1,2,\ldots,$ and solve these ordinary-differential equations using standard methods. This approach only works for memory functions of this type. Approximate solutions were obtained using $g=7/[(n-l)\Delta u]^2$. For negative u, we set $W(u)=W(|u|)$.

The negative logarithm of the absolute error in $q(t)$,

$$\epsilon(t)=-\log_{10}|q(t)-q_{\mathrm{approx.}}(t)|, \tag{18}$$

is shown in Fig. 3 plotted against time for the values of n indicated in the inset. [The error in $p(t)$ is similar.] As n

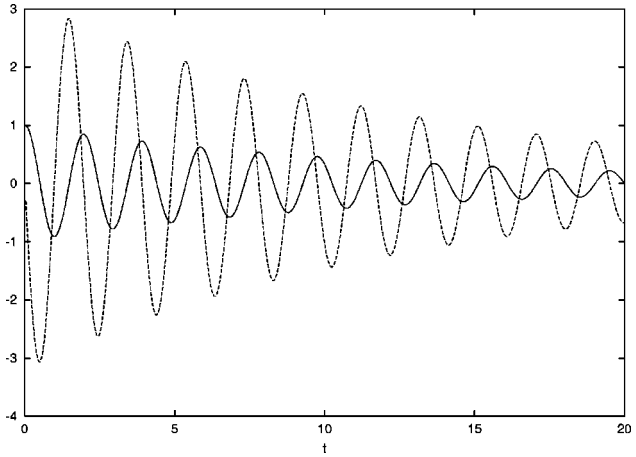

FIG. 2. Position (solid curve) and momentum (dashed curve) of a damped oscillator.

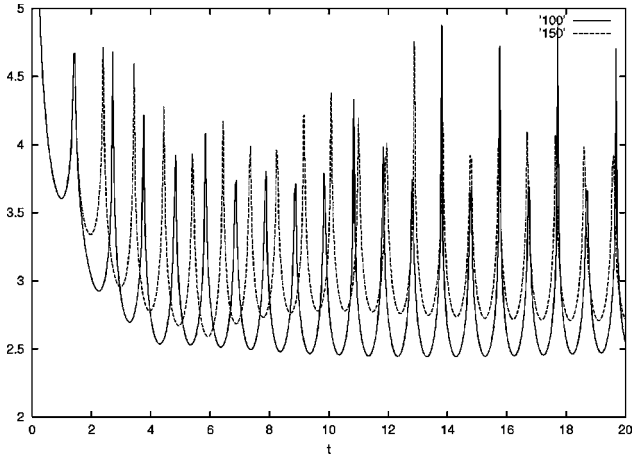

FIG. 3. $\epsilon(t)$ for memory function (12).

increases, ϵ increases (on average) and hence the error decreases. The oscillations in ϵ are caused by periodic intersections of the two solutions. In practice, it is impossible to visually distinguish the two solutions when $\epsilon \geqslant 2$. Note that after a short transient the error (on average) does not increase. This is probably a consequence of the linearity of these equations. Some decline in accuracy with time should be expected when the Langevin equations are nonlinear (e.g., a particle in a double well).

Figure 4 compares the exact solutions for $q(t)$ (solid curve) and $p(t)$ (short-dashed curve) with those obtained using our method for $n=150$ (dashed and dotted curves, respectively) over a time of 40 units. No disagreement is visible. Convergence for memory function (13) is similar.

Memory functions (14) and (15) that take negative values and have long time tails require many grid points for convergence. Figure 5 shows the negative logarithm (base 10) of the absolute error in $q(t)$ for this case. While many grid points are required, high accuracy solutions can clearly be obtained using our method.

For the master equation, we chose an initial value problem consisting of a dissipative two-level system representing a spin interacting with environmental degrees of freedom. If

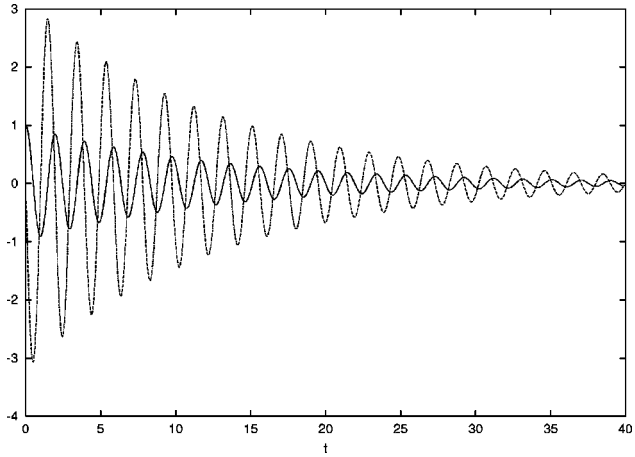

FIG. 4. Comparison of exact and approximate position and momentum of a damped oscillator.

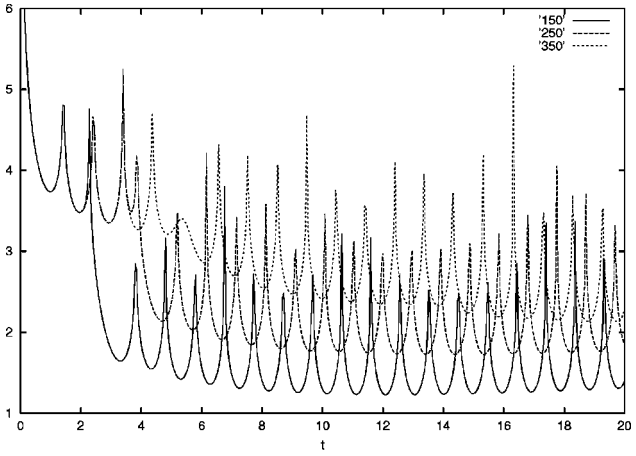

FIG. 5. $\epsilon(t)$ for memory function (14).

the spin Hamiltonian is $H=(\omega/2)\sigma_z+\beta\sigma_x$ and the coupling to the environment is proportional to σ_x, then the equation for the density matrix $\rho(t)$ is of the form [3,4]

$$\frac{d\rho(t)}{dt}=-i\left[\frac{\omega}{2}\sigma_z+\beta\sigma_x,\rho(t)\right]-C\int_0^t W(t-t')\{\sigma_x^2\rho(t') + \rho(t')\sigma_x^2-2\sigma_x\rho(t')\sigma_x\}\ dt', \tag{19}$$

where the σ's denote Pauli matrices. Parameters were set as $\omega=1=\beta$ and $C=0.2$. We chose to define $\chi(t,u)=\int_0^t W(t-t')\rho(t')dt'$, which differs somewhat from the general definition employed in Eq. (7). The transformed equations are then

$$\frac{d\rho(t)}{dt}=-i\left[\frac{\omega}{2}\sigma_z+\beta\sigma_x,\rho(t)\right]-2C\{\chi(t,0)-\sigma_x\chi(t,0)\sigma_x\}, \tag{20}$$

$$\frac{d\chi(t,u)}{dt}=e^{-gu^2}W(u)\rho(t)+\frac{\partial\chi(t,u)}{\partial u}+2gu\ \ \chi(t,u). \tag{21}$$

Theory predicts that the memory function $W(t)$ for this problem is approximately Gaussian in form [4]. However, we were unable to obtain an exact solution of the master equation for this case [11]. Instead we approximate the Gaussian via the similar function $W(t)=14e^{-7.4t}-13e^{-8t}$. Exact solutions for

$$\langle\sigma_z\rangle(t)=\mathrm{Tr}\{\sigma_z\rho(t)\}=\rho_{11}(t)-\rho_{00}(t)\quad\text{(solid curve)}, \tag{22}$$

$$\langle\sigma_x\rangle(t)=\mathrm{Tr}\{\sigma_x\rho(t)\}=\rho_{10}(t)+\rho_{01}(t)\quad\text{(dashed curve)}, \tag{23}$$

$$\langle\sigma_y\rangle(t)=\mathrm{Tr}\{\sigma_y\rho(t)\} =i(\rho_{10}(t)-\rho_{01}(t))\quad\text{(short-dashed curve)}, \tag{24}$$

and initial conditions $\langle\sigma_z\rangle(0)=1$ and $\langle\sigma_x\rangle(0)=0=\langle\sigma_y\rangle(0)$ were obtained in the same way as for the gener-

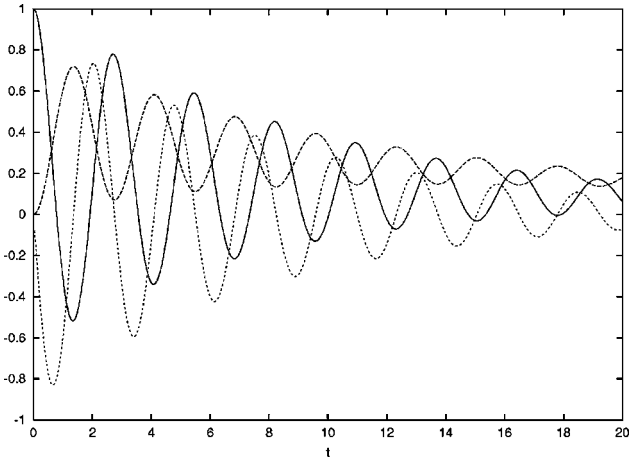

FIG. 6. Spin x (solid curve), y (dashed curve), and z (short-dashed curve) components.

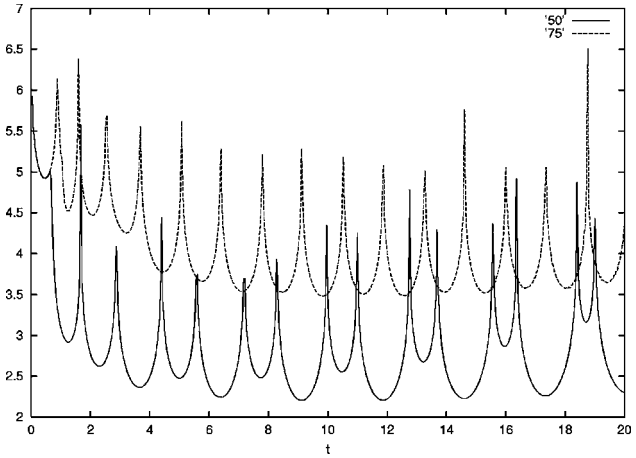

FIG. 7. $\epsilon(t)$ for $\langle \sigma_z \rangle$.

alized Langevin equations and are plotted versus time in Fig. 6. For the approximate method we used $g=11/[(n-l)\Delta u]^2$, and for negative u, we set $W(u)=W(|u|)$. From Fig. 7, where we plot

$$\epsilon(t) = -\log_{10}|\langle \sigma_z \rangle(t) - \langle \sigma_z \rangle_{\text{approx.}}(t)| \tag{25}$$

against time, we see that convergence of the numerical method is very rapid for these equations. (Similar accuracies are achieved for $\langle \sigma_x \rangle$ and $\langle \sigma_y \rangle$.)

Thus, we have shown that accurate solutions of integro-differential equations can be obtained via transformation to a larger set of ordinary-differential equations. Because this transformation is exact, we expect that the method will also work for equations not considered in this paper. It should be possible to obtain accurate solutions for such equations via the following steps. First, find an approximation of the memory function or operator that will allow exact solutions to be obtained. Second, optimize the numerical method by finding the best g for the model equations. Finally, apply the numerical method to the original equations and look for convergence of the solutions with increasing n.

The author gratefully acknowledges the financial support of the Natural Sciences and Engineering Research Council of Canada.

[1] See, for example, G. Frenkel and M. Schwartz, Europhys. Lett. **50**, 628 (2000).
[2] C. Meier and D.J. Tannor, J. Chem. Phys. **111**, 3365 (1999).
[3] J. Wilkie, J. Chem. Phys. **114**, 7736 (2001).
[4] J. Wilkie, J. Chem. Phys. **115**, 10 335 (2001).
[5] W.H. Press, S.A. Teukolsky, W.T. Vetterling, and B.P. Flannery, *Numerical Recipes in FORTRAN 77*, 2nd ed. (Cambridge University Press, Cambridge, 2001).
[6] U. Peskin and N. Moiseyev, J. Chem. Phys. **99**, 4590 (1993); P. Pfeifer and R.D. Levine, *ibid.* **79**, 5512 (1983).
[7] J. Wilkie, Phys. Rev. E **62**, 8808 (2000); G. Chen and R. Grimmer, J. Diff. Eqns. **45**, 53 (1982).
[8] S. Shaw and J.R. Whiteman, Comput. Methods Appl. Mech. Eng. **150**, 397 (1997); R.C.Y. Chin, G.W. Hedstrom, and G. Majda, Geophys. J. R. Astron. Soc. **86**, 137 (1986).
[9] D.T. Colbert and W.H. Miller, J. Chem. Phys. **96**, 1982 (1992).
[10] E. Hairer and G. Wanner, http://elib.zib.de/pub/elib/hairer-wanner/nonstiff/
[11] Laplace transforms of the exact solutions are readily obtained but inverting the transform is problematic.